#5616

Crystal Structure of Drug-resistant ROS1 G2032R in Complex with Zidesamtinib, a Clinical-stage ROS1 Inhibitor with Best-in-class Potential

Joseph Magrino[1], Anupong Tangpeerachaikul[1], Scot Mente[1], Henry E. Pelish[1]

[1] Nuvalent, Cambridge, MA, United States

ZIDESAMTINIB DEVELOPMENT RATIONALE

Zidesamtinib (NVL-520) is a ROS1 tyrosine kinase inhibitor (TKI) created with the aim to overcome the limitations of currently available ROS1 TKIs by maintaining activity against ROS1 resistance mutations, having brain penetrance, and avoiding TRK inhibition (Figure 1).[1–3]

TKI:	Crizotinib	Entrectinib	Lorlatinib	Repotrectinib	Taletrectinib	Zidesamtinib
Status* for *ROS1+* NSCLC:	Approved	Approved	Investigational	Approved	Investigational#	Investigational

Zidesamtinib Design Goals

1	Activity against ROS1	ROS1 fusions are oncogenic drivers in various cancers, including 1 – 3% of NSCLC[1]
2	Activity against ROS1 mutations	ROS1 G2032R develops after progression on crizotinib (~40%), entrectinib, & lorlatinib[4]
3	Brain penetrance	Brain metastases are the site of progression in ~50% of patients receiving crizotinib[5]
4	Avoiding TRK-related neurotoxicities	TRK inhibition in CNS is linked to neurologic adverse events and dose-limiting toxicities[6]

▲ **Figure 1 | Zidesamtinib development rationale.** Also see Disclaimer. *US FDA approval status as of April 1, 2025. #Taletrectinib is approved for *ROS1+* NSCLC in China, with an NDA under priority review with the US FDA as of April 1, 2025.

2.2 Å CRYSTAL STRUCTURE OF ROS1 G2032R + ZIDESAMTINIB

▲ **Figure 2 | Crystal structure of zidesamtinib bound to ROS1 G2032R (PDB:9QEK).**

- ROS1 G2032R kinase domain expressed in Sf21 cells was purified by tandem His and size-exclusion chromatography and crystallized in the presence of zidesamtinib via sitting-drop vapor diffusion over 39 days.
- The structure was solved by Molecular Replacement using XDS, Pointless, & STARANISO to 2.2 Å resolution (Figure 2 & Table 1).[4–10]
- Zidesamtinib binds to the ROS1 G2032R ATP-binding pocket.

Data collection statistics		Structure refinement statistics	
Space group	$P6_4$	# Reflections	11767
Resolution (Å)	34.70–2.21	# Atoms	2290
# Unique reflections	12138	Average B factor (Å^2)	66.20
I/σ(I)	11.2	R_{work}	0.202
Multiplicity	7.6	R_{free}	0.269
R_{merge}	0.08	r.m.s.d. bonds (Å)	0.012
R_{meas}	0.10	r.m.s.d. angles (°)	1.1858
R_{pim}	0.05		
CC(1/2)	1.00		

▲ **Table 1 | Crystal and structure refinement statistics.**

BIOCHEMICAL CHARACTERIZATION

- The ATP-binding pocket remained largely unchanged in both polarity and size between ROS1 and ROS1 G2032R, and docking indicated that the G2032R mutation is unlikely to impede ATP binding (Figure 3).
- Recombinant ROS1 displayed slightly higher catalytic efficiency than ROS1 G2032R but similar Michaelis constants for ATP, suggesting that the ROS1 G2032R mutant maintains kinase activity and ATP binding (Table 2).
- Zidesamtinib maintains IC_{50} < 10 nM against ROS1 G2032R in the biochemical kinase assay, whereas repotrectinib and taletrectinib have IC_{50} = 30 and 100 nM, respectively (Table 2).[1]

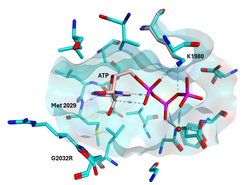

▲ **Figure 3 | Modeling of ATP in the binding pocket of ROS1 G2032R crystal structure.** ATP structure based on PDB:4GT3.

	ROS1	ROS1 G2032R
Michaelis Menten kinetics with ATP titration		
V_{max} (RFU/min)	192 ± 2.7	157 ± 1.5
K_m (μmol/L)	24.6 ± 1.3	14 ± 0.6
k_{cat} (s^{-1})	640	105
k_{cat}/K_m (L μmol^{-1} s^{-1})	26	7.5
Biochemical potency (IC_{50})		
Zidesamtinib	**0.7 nM**	**7.9 nM**
Repotrectinib	1.3 nM	30 nM
Taletrectinib	1.8 nM	100 nM

▲ **Table 2 | Biochemical characterization of ROS1 and ROS1 G2032R.** Some Michaelis-Menten kinetics parameters shown as mean ± SEM.

MOLECULAR INTERACTION BETWEEN ZIDESAMTINIB AND ROS1 G2032R

HINGE & OTHER INTERACTIONS

- Zidesamtinib fills the entire ATP binding pocket of ROS1 G2032R (Figure 4A).
- The aminopyridine forms two canonical hydrogen bonds with residues E2027 and M2029 in the hinge region (Figure 4B).
- The fluorobenzene inserts into a shallow cavity at the floor of the pocket, positioning the ortho-hydrogen atom for interaction with the carbonyl of R2083 (Figure 4C).
- CH-π interactions were observed between the R2032 sidechain and the π-system of the *N*-ethylpyrazole, and between the terminal methyl groups of L2086 and the π-systems of the aminopyridine and fluorobenzene moieties (Figure 4C).

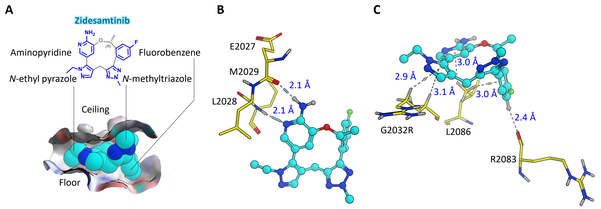

▲ **Figure 4 | Structural analysis illuminates binding of zidesamtinib with ROS1 G2032R. A.** Each region of zidesamtinib complements the shape of the ROS1 G2032R ATP binding pocket. **B–C.** Hinge (C) and other (D) intermolecular interactions.

P-LOOP STABILIZATION

- Overlay of ROS1 G2032R and wild-type ROS1 crystal structures indicated high similarity, with average α-carbon root-mean-square deviation (RMSD) of 0.6 Å (Figure 5A).[4,11,12]
- The P-loop of ROS1 G2032R bound to zidesamtinib (PDB:9QEK) is shifted ~1.5 Å upward compared to wild-type ROS1 bound to lorlatinib (PDB:4UXL) (Figure 5B) and displays a lower B-factor (Figure 5C).
- This suggests that the *N*-methyltriazole group of zidesamtinib may reduce the P-loop's degrees of freedom and lock it in this crystallographic state.

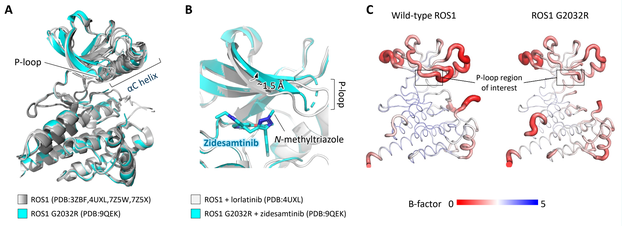

▲ **Figure 5 | P-loop differences between wild-type ROS1 and ROS1 G2032R. A.** ROS1 & ROS1 G2032R overlayed. **B.** P-loop shifts upward for ROS1 G2032R compared to wild-type ROS1, suggesting potential interaction with zidesamtinib's *N*-methyltriazole. **C.** B-factor analysis shows rigidification of the p-loop region of interest, boxed, in ROS1 G2032R compared to wild-type ROS1.

CONFORMATIONAL ANALYSIS & MOLECULAR DYNAMICS

- The α and β carbon atoms of R2032 adopt a gauche$^+$ conformation (χ1 angle = 306°), allowing it to engage in multiple CH-π interactions with the *N*-ethylpyrazole ring of zidesamtinib (Figure 6A).[13]
- Overlay of ROS1-bound lorlatinib (PDB:4UXL)[10] and crizotinib (PDB:3ZBF)[4] crystal structures onto our ROS1 G2032R protein structure indicated potential steric clashes between these TKIs and R2032 (Figure 6B).
- Molecular dynamics simulations revealed that R2032 adopts the energetically more favorable gauche$^+$ conformation with zidesamtinib, forming favorable hydrogen-bond interactions in some frames (Figure 6C).
- By contrast, R2032 adopts the energetically less favorable gauche$^-$ conformation with lorlatinib, which may contribute to its potency loss against ROS1 G2032R (Figure 6C).

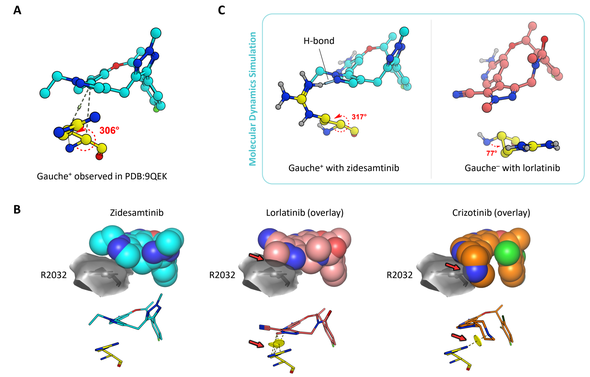

▲ **Figure 6 | Structural impact of G2032R mutation on TKI binding. A.** R2032 adopts a gauche$^+$ conformation with zidesamtinib in the crystal structure. **B.** Overlay of existing ROS1-bound lorlatinib (PDB:4UXL) and crizotinib (PDB:3ZBF) structures on our ROS1 G2032R structure (PDB:9QEK) reveals steric clashes with the R2032 residue, indicated with red arrows. **C.** Molecular dynamics simulations reveal a gauche$^+$ R2032 conformation for zidesamtinib but a gauche$^-$ R2032 conformation for lorlatinib.

FREE ENERGY PERTURBATION PREDICTS BINDING AFFINITY

- Free Energy Perturbation (FEP) is a method that employs all-atom and explicit solvent molecular dynamics to compute the free energies between two different states. We applied FEP to study the impact of the G2032R modification on TKI affinity (Figure 7A).[14–18]
- In a set of 6 approved or investigational ROS1 TKIs, FEP predicted affinity changes ($\Delta\Delta G_{FEP}$) that correlated well with reported experimental data ($\Delta\Delta G_{biochem}$) (Figure 7B). Zidesamtinib and repotrectinib clustered toward the bottom-left corner of the correlation plot, consistent with tolerance for the G2032R mutation imparted by minimal steric bulk in the solvent-front region. By contrast, crizotinib, entrectinib, and lorlatinib clustered toward the top-right corner, consistent with G2032R resistance imparted by steric clashes.
- While FEP predictions were often similar in both G → R and R → G directions, differences were observed for repotrectinib and crizotinib, indicating that the two directions were reciprocal but not necessarily identical (Figure 7B).

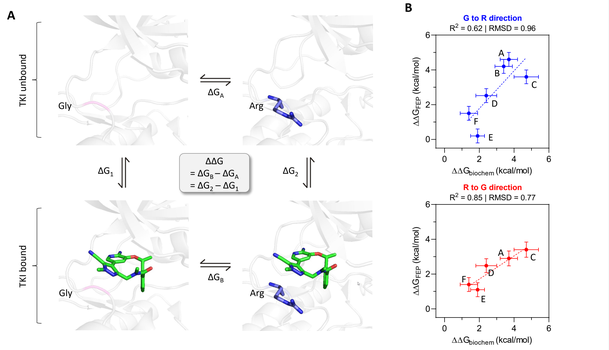

Figure 7 | Free-energy perturbation (FEP) calculations predict potency changes due to G-to-R mutation. A. Thermodynamic cycle involves free energies of the glycine to arginine mutation (ΔG_A and ΔG_B) and of TKI binding (ΔG_1 and ΔG_2), with lorlatinib shown as an example. ΔΔG denotes predicted change in binding free energy caused by the G2032R mutation. **B.** Experimental ($\Delta\Delta G_{biochem}$) and predicted ($\Delta\Delta G_{FEP}$) changes in binding free energy for each ROS1 TKI shown as mean ± SEM with A=crizotinib, B=entrectinib, C=lorlatinib, D=taletrectinib, E=repotrectinib, and F=zidesamtinib. R^2 denotes correlation coefficient, and RMSD denotes the root-mean-squared deviation.

ZIDESAMTINIB SPARES TRKB

- Zidesamtinib was designed to spare inhibition of TRK-family kinases by sterically clashing with the key differentiating residue Y591 on TRKA and Y619 on TRKB/TRKC, analogous to the smaller residue L2028 on ROS1 (Figure 8).[3,12]
- Overlay of the zidesamtinib-bound ROS1 G2032R structure onto the repotrectinib-bound TRKA structure indicated that zidesamtinib's *N*-ethylpyrazole clashed with TRKA Y591 but accommodated ROS1 L2028, consistent with its selective inhibition.[19]
- Repotrectinib showed no clash with either ROS1 or TRKA, consistent with its dual TRK/ROS1 inhibitory design and with reported TRK-related adverse events.[20]

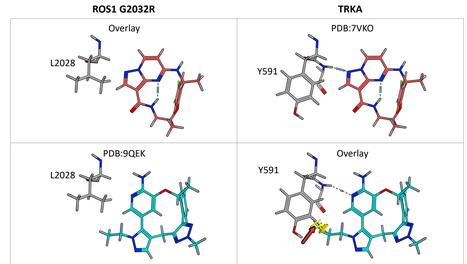

Figure 8 | Structural basis for TRK selectivity. (Top) Overlay of ROS1-bound repotrectinib (PDB:7VKO) on ROS1 G2032R or TRKA indicates no clash with either protein, suggesting potential binding to both. (Bottom) Overlay of ROS1 G2032R-bound zidesamtinib on TRKA indicates clashing with Y591, suggesting potentially selective binding to ROS1 G2032R over TRK-family kinases.

CONCLUSIONS

- Preclinical data suggest that zidesamtinib has a differentiated profile that combines activity against ROS1 resistance mutations, brain penetrance, and TRK avoidance[1,2].
- **Our crystal structure provides an explanation for zidesamtinib's high affinity for ROS1 G2032R and selectivity for ROS1 over TRK:**
  - Favorable binding of zidesamtinib to ROS1 G2032R through key interactions with the hinge, floor, and ceiling (p-loop) within the ATP-binding pocket.
  - MD simulations indicated a favorable R2032 gauche$^+$ conformation bound to zidesamtinib.
  - Two-way FEP calculations suggested that zidesamtinib can maintain activity against ROS1 G2032R.
  - Overlay of ROS1 and TRK structures revealed potential steric clashes between zidesamtinib and TRKA Y591, suggesting selective binding to ROS1 over TRK-family kinases.
- Our crystal structure provides additional validation for the FEP methodology, which accurately predicted affinity changes caused by ROS1 G2032R across TKIs with diverse chemotypes. This highlights the potential of FEP for interrogating novel binders targeting solvent-front mutant kinases.
- To our knowledge, this represents the first structure of ROS1 G2032R or any mutant ROS1 reported.

Abbreviations

ATP = Adenosine triphosphate
CNS = Central nervous system
FDA = Food and Drug Administration
FEP = Free-energy perturbation
MD = Molecular dynamics
NSCLC = Non-small cell lung cancer
PDB = The Protein Data Bank
RMSD = Root Mean Square Deviation
ROS1+ = *ROS1*-positive (cancers)
SEM = Standard error of the mean
TKI = Tyrosine kinase inhibitors
ΔG = Free energy (of binding)
$\Delta\Delta G_{FEP}$ = Differences in FEP-calculated ΔG
$\Delta\Delta G_{biochem}$ = Differences in experimental ΔG

Disclaimer

As of March 2025, crizotinib, entrectinib, and repotrectinib have been approved by the FDA for the treatment of patients with *ROS1+* metastatic NSCLC. **Zidesamtinib is being investigated in a Phase 1/2 trial for patients with advanced *ROS1+* NSCLC and other solid tumors (ARROS1, NCT05118789).** No head-to-head clinical studies have been conducted for zidesamtinib against any approved or investigational therapies. Preclinical experiments are not powered to determine the statistical significance of differences in measurements between any of the inhibitors tested.

References

1. Drilon et al. Nat Rev Clin Oncol 2021;18:35–55.
2. Lin et al. J Thorac Oncol 2017;12:1611–25.
3. Drilon et al. Cancer Discov 2023;13:598–615.
4. Kabsch W. XDS. Biol Crystallogr 2010;66:125–32.
5. Awad et al. N Engl J Med 2013;368:2395–401.
6. Evans P. D Biol Crystallogr 2006;62:72–82.
7. Evans PR. D Biol Crystallogr 2011;67:282–92.
8. Tickle et al. STARNISO 2016.
9. Vagin et al. D Biol Crystallogr 2004;60:2184–95.
10. Zou et al. PNAS 2015; 112(11) 3493-8
11. Petrovič D et al. J Chem Inf Model 2022;62:3832–43.
12. Murray et al. Mol Cancer Ther 2021;20:2446–56.
13. Janin et al. J Mol Biol 1978;125:357–86.
14. Wang L et al. Field. J Am Chem 2015;137:2695–703.
15. Abel R et al. Acc Chem Res 2017;50:1625–32.
16. Yu. J Chem Theory Comput. 2017;13:6290–30
17. Kuhn et al. American Chemical 2017;60:2485–97.
18. Wang et al. J Chem Theory Comput. 2017;13:42–54.
19. Murray et al. Mol Can Ther 2021; 20 (12):2446-2456
20. Drilon et al. NEJM 2024; 390 (2); 118-131

Financial Disclosures: JM, AT, SM, and HEP report employment with and ownership interest in Nuvalent.

Correspondence: info@nuvalent.com